In-plane loaded CLT beams – Tests and analysis of element lay-up

Danielsson, Henrik; Serrano, Erik; Jeleč, Mario; Rajčić, Vlatka

Published in:
International Network on Timber Engineering Research - Proceedings Meeting 50

2017

Document Version:
Publisher's PDF, also known as Version of record

In-plane loaded CLT beams – Tests and analysis of element lay-up

Henrik Danielsson, Division of Structural Mechanics, Lund University, Sweden

Erik Serrano, Division of Structural Mechanics, Lund University, Sweden

Mario Jeleč, Department of Materials and Structures, University of Osijek, Croatia

Vlatka Rajčić, Department of Structures, University of Zagreb, Croatia

Keywords: CLT, testing, in-plane loading, beam, hole, notch

1 Background, aim and objectives

This work concerns in-plane loaded CLT beams, including beams with a hole or a notch. Using CLT for such structural elements is very relevant from a practical engineering point of view since the transversal layers have a reinforcing effect with respect to stress perpendicular to the beam axis.

Due to the general composition of CLT, the stress state is however very complex and many failure modes need to be considered in design. The beam strength is furthermore affected not only by the basic material strength and the gross cross sections dimensions, but also affected by the ratio of the longitudinal and transversal layer widths and by the dimensions of the cross sections of the individual laminations. Many of the geometry parameters are defined by the producer, e.g. the widths t_0 and t_{90} of the longitudinal and transversal layers respectively. Other parameters, such as dimensions of individual laminations and lamination placement with respect to element edges, are often not known to the engineer in an actual design situation since the beams in general are cut from larger elements. In this cutting, no consideration of the location of the beam element edges in relation to the edges of the individual laminations is made.

Experimental tests on CLT beams are for example reported by Bejtka (2011) and Andreolli et al (2012). Comprehensive experimental tests and a composite beam model for stress analysis and strength verification have further been presented by Flaig (2013, 2014, 2015a, 2015b) and by Flaig and Blass (2013), including stress based failure criteria for relevant failure modes. A basic assumption for that model is that the CLT lay-up

for 5-layer elements consists of an interior longitudinal layer of twice the width as compared to the width of the surface layers (e.g. an interior longitudinal layer composed of two, flatwise glued, longitudinal laminations). The tests were also mostly carried out on beam specimens having this type of lay-up, which is relevant from an academic point of view but less relevant from a practical point of view since this type of lay-up very seldom is used in practice. Most specimens were furthermore produced with a regular lamination pattern having *m* number of laminations of equal width *b* in the longitudinal layers, i.e. total beam height $h = mb$.

The aim of this paper is to present a base for verification of the model for stress and strength analysis suggested by Flaig (2015a, 2015b). Of the many lay-up parameters influencing CLT-beam behaviour, this paper focuses on the effect of interior longitudinal layer width and the resulting magnitude and distribution of internal forces in the beam and the torsional moments acting in the crossing areas.

2 Tests of in-plane loaded CLT beam elements

Tests on in-plane loaded CLT beams have been carried out at Lund University and a detailed description of the tests and results are presented in Danielsson et al (2017).

Five different test setups A-E according to Figure 2.1 were used. Each test series consisted of four nominally equal tests giving a total of 20 individual tests. The beams were produced from symmetrical 5-layer CLT and had a height of h = 600 mm and a gross cross section width of 160 mm (40-20-40-20-40). Each of the three longitudinal layers had a layer thickness of 40 mm and both transversal layers had a thickness of 20 mm. The laminations used for the longitudinal and transversal layers were of 172 mm and 146 mm width, respectively.

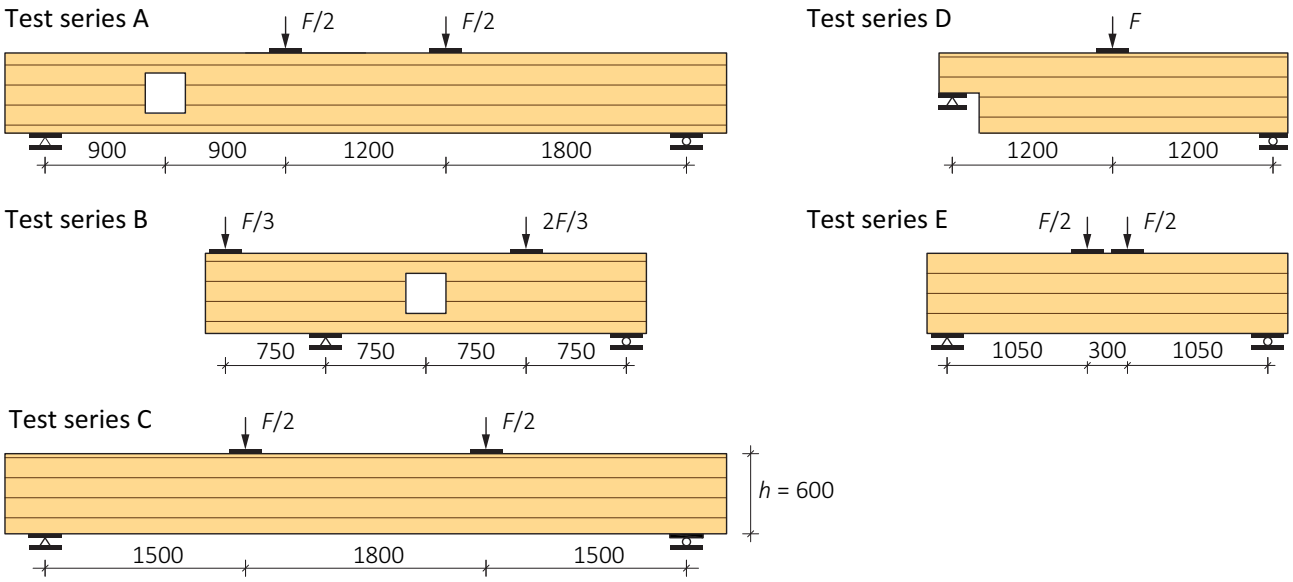

Figure 2.1. Overview of test series for in-plane loaded CLT beams, dimensions in mm.

For test series A and B, a square hole of side length 300 mm was placed centrically with respect to the beam height direction. For the test series D, a notch of depth 300 mm was used and the centreline of the support was placed at a distance of 200 mm from the notched corner. Holes and notches were cut by the manufacturer without corner radius.

All beams were produced by Cross Timber Systems Ltd according to the European Technical Assessment ETA-15/0906 (2016). The wood species used is stated as being European spruce or equivalent softwood. The mean density of the test specimens was 456 kg/m^3 and the moisture content at the time of testing was 10-11 %. It is in the ETA stated that the narrow faces of the laminations belonging to the same layer need not to be bonded together. At the time of testing, there were no visible gaps between the laminations in the elements and there appear not to have been any (or very little) edge-bonding between the laminations.

Compared to the experimental tests presented by Flaig (2013), the present tests concern elements of more conventional CLT lay-up: equal width of all longitudinal layers. The specimens were furthermore cut from larger CLT panels, meaning that the widths of the upper- and lower-most longitudinal laminations were random in the range 5 mm < b < $b_{max,}$ where b_{max} = 172 mm. Also the placement of holes and notches was random with respect to the position of the longitudinal and transversal laminations.

3 Analytical beam models

Models for stress analysis and beam strength verification for in-plane loading of CLT elements are for example presented by Flaig (2013, 2014, 2015a, 2015b) and by Flaig and Blass (2013). These models are in general based on conventional beam theory considerations with addition of certain assumptions and simplifications to account for the orthogonal layered composition.

3.1 Prismatic beams

A brief review of the model for calculation of stresses relating to the relevant failure modes is presented below. The equations presented are based on models by Flaig (2013, 2014, 2015a, 2015b) and by Flaig and Blass (2013). The equations are based on notation for geometry and load parameters according to Figures 3.1 and 3.2 and relate to prismatic CLT beams without edge-bonding and composed of laminations having identical stiffness properties. A more detailed review of the considered model is presented in Danielsson et al (2017).

The maximum normal stress in the longitudinal layers, due to bending, is given by

$$\sigma_{\mathrm{x}} = \frac{M}{W_{\mathrm{net}}} \qquad \text{where} \quad W_{\mathrm{net}} = \frac{t_{\mathrm{net},0} h^2}{6} \tag{1}$$

where M is the bending moment, $t_{net,0} = \Sigma t_{0,k}$ and h is the beam height.

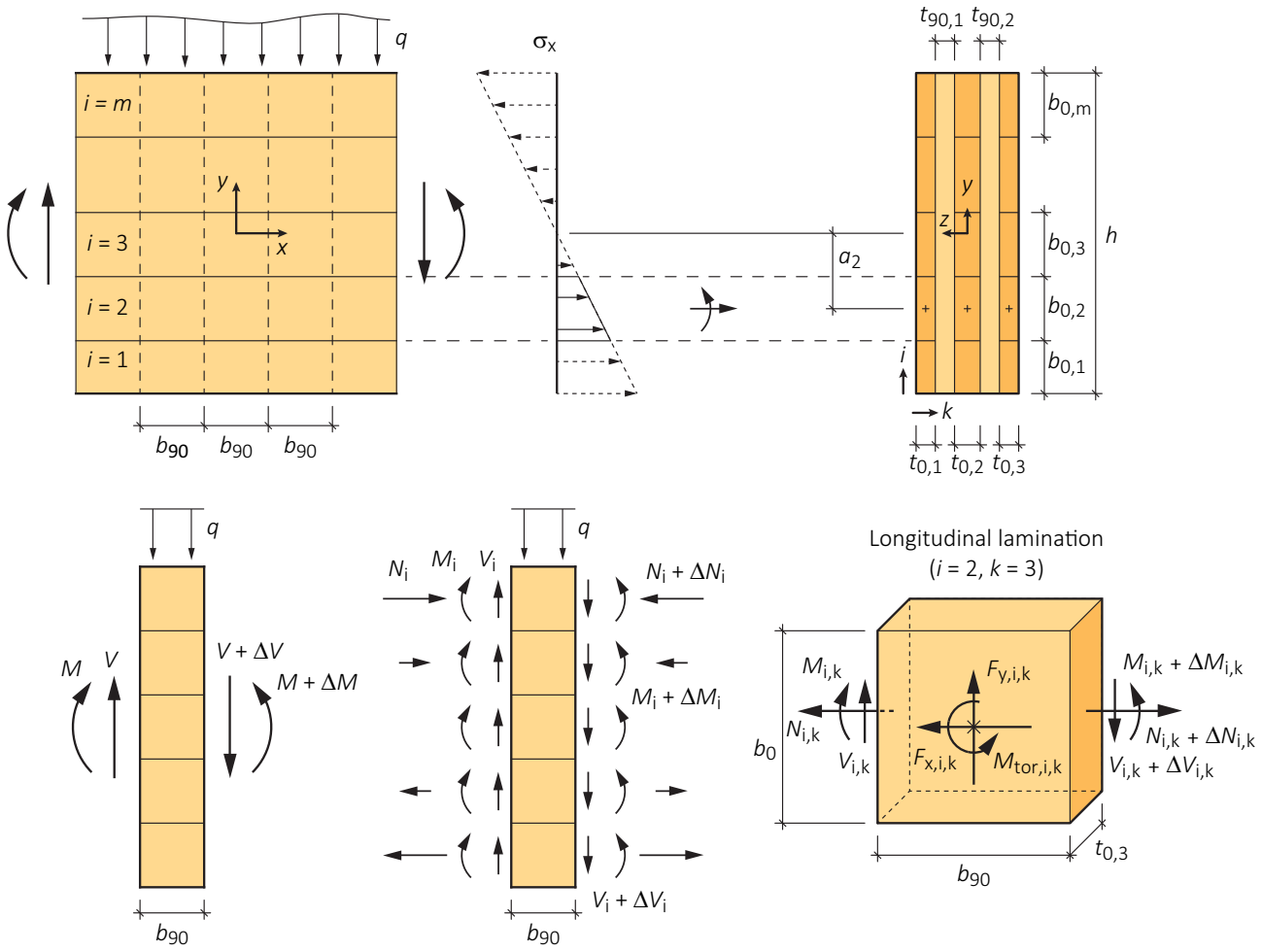

Figure 3.1. Illustration of beam model and definition of load and geometry parameters.

The maximum value of the gross shear stress (shear failure mode I) is given by

$$\tau_{xy,gross} = \frac{3}{2}\frac{V}{t_{gross}h} \qquad (2)$$

where V is the shear force and $t_{gross} = \Sigma t_{0,k} + \Sigma t_{90,k}$ is the gross cross section width.

The maximum value of the net shear stress in the longitudinal and transversal layers (shear failure mode II) are given by

$$\tau_{xy,net,0} = \frac{3}{2}\frac{V}{t_{net,0}h} \quad \text{and} \quad \tau_{xy,net,90} = \frac{3}{2}\frac{V}{t_{net,90}h} \qquad (3, 4)$$

where $t_{net,0} = \Sigma t_{0,k}$ and $t_{net,90} = \Sigma t_{90,k}$ refer to the net cross section width of the longitudinal and transversal layers, respectively.

In addition to the shear stress τ_{xy}, which are present in both longitudinal and transversal laminations, shear stresses τ_{xz} and τ_{yz} acting in the crossing areas between the longitudinal and transversal laminations are also present. Using the model as suggested by Flaig, the shear stresses acting in the crossing area can be categorized as (a) shear stress parallel to the beam axis τ_{xz}, (b) shear stress perpendicular to the beam axis τ_{yz} and (c) torsional shear stress τ_{tor}.

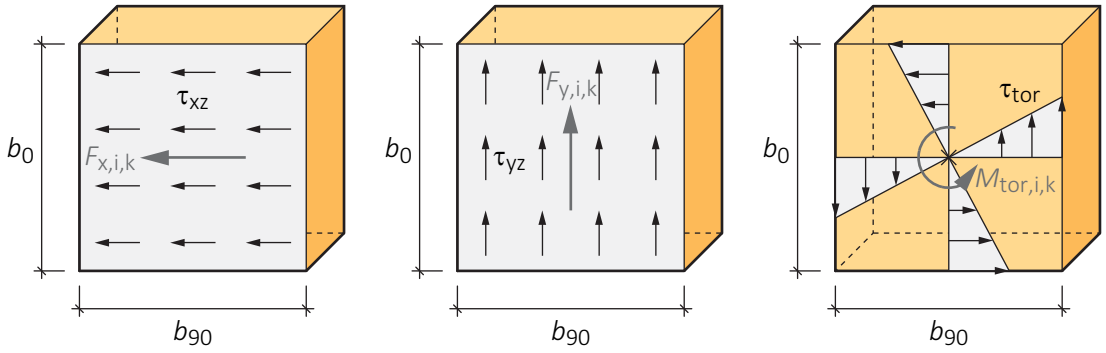

Figure 3.2. Illustration of assumed shear stress distributions in the crossing areas.

The distributions of the shear stresses over the crossing areas are assumed according to the illustration in Figure 3.2 and the derivation of maximum stress values are based on calculation of the forces $F_{x,i,k}$ and $F_{y,i,k}$ and the torsional moment $M_{tor,i,k}$ acting in the crossing area *i*,*k* according to Figure 3.1.

The shear stress τ_{xz} in the crossing area/areas belonging to lamination *i*,*k* is given by

$$\tau_{\mathrm{xz,i,k}} = \frac{F_{\mathrm{x,i,k}}}{b_{0,\mathrm{i}} b_{90}} \qquad \text{where} \qquad F_{\mathrm{x,i,k}} = \frac{\Delta N_{\mathrm{i,k}}}{n_{\mathrm{CA,k}}} \tag{5}$$

where $\Delta N_{i,k}$ is the differential normal force in longitudinal lamination *i* of layer *k*, $n_{CA,k}$ is the number of crossing areas that longitudinal lamination *i*,*k* shares with adjacent transversal laminations and $b_{0,i}$ and b_{90} are the widths of the longitudinal and transversal laminations, respectively. The differential normal force $\Delta N_{i,k}$ can be expressed as

$$\Delta N_{\mathrm{i,k}} = \frac{\Delta M}{I_{\mathrm{net}}} t_{0,\mathrm{k}} b_{0,\mathrm{i}} a_{\mathrm{i}} \tag{6}$$

where $\Delta M = V b_{90}$. Assuming equal width of the transversal and longitudinal laminations (i.e. $b_0 = b_{90} = b$) and constant ratio between the longitudinal layer widths and the number of crossing areas for each layer (i.e. constant value of $t_{0,k}/n_{CA,k}$), the maximum value of the shear stress parallel to the beam axis may then be expressed as

$$\tau_{\mathrm{xz}} = \frac{6V}{b^2 n_{\mathrm{CA}}} \left(\frac{1}{m^2} - \frac{1}{m^3} \right) \tag{7}$$

where n_{CA} is the total number of crossing areas in the beam width direction and *m* is the number on longitudinal laminations in the beam height direction (i.e. $m = h/b$).

The shear stress perpendicular to the beam axis, from a distributed load *q* [N/m] caused by e.g. a distributed support reaction force, may be expressed as

$$\tau_{\mathrm{yz}} = \frac{q}{h n_{\mathrm{CA}}} \tag{8}$$

The torsional shear stress distribution illustrated in Figure 3.2, and corresponding to relative rigid body rotation over a shear compliant medium, gives a maximum torsional shear stress of the middle points of the four sides according to

$$\tau_{\mathrm{tor,i,k}} = \frac{M_{\mathrm{tor,i,k}}}{I_{\mathrm{P,CA,i,k}}} \frac{b_{\mathrm{max}}}{2} \qquad \text{where} \qquad I_{\mathrm{P,CA,i,k}} = \frac{b_{0,\mathrm{i}} b_{90}}{12} \left(b_{0,\mathrm{i}}^2 + b_{90}^2 \right) \tag{9}$$

where b_{max} = max($b_{0,i}$, b_{90}). Assuming b_0 = b_{90} = b, constant value of $t_{0,k}/n_{CA,k}$ and equal torsional moments for all crossing areas in the beam height direction, the maximum torsional shear stress may then be expressed as

$$\tau_{\mathrm{tor}} = \frac{3V}{b^2 n_{\mathrm{CA}}}\left(\frac{1}{m} - \frac{1}{m^3}\right) \qquad (10)$$

3.2 Beams with a hole or an end-notch

For CLT beams with a hole or an end-notch, failure modes relating to bending at the hole/notch and tension perpendicular to the beam axis are also relevant, in addition to the failure modes mentioned in Section 3.1. Proposals for design equations are presented by Flaig (2015b), see also Jeleč et al (2016).

3.3 Shear strengths and stress interaction criteria for failure in crossing areas

For verification with respect to gross shear failure (mode I), characteristic shear strength according to the strength class of the laminations according to EN 338 and use of k_{cr} = 1.0 is proposed by Flaig (2015a). For net shear failure (mode II), a characteristic shear strength of 8.0 MPa is suggested.

Regarding shear failure in the crossing areas (shear failure mode III), the three stress components reviewed above (τ_{xz}, τ_{yz} and τ_{tor}) represent for a specific point either longitudinal shear, rolling shear or a combination of both. A shear stress component giving pure longitudinal shear in the longitudinal lamination represents pure rolling shear in the transversal laminations, and vice versa. Thus, for failure in the crossing areas, and based on experimental tests on crossing areas loaded in either uniaxial shear, pure torsion, or a combination of both, failure criteria according to

$$\frac{\tau_{\mathrm{tor}}}{f_{\mathrm{v,tor}}} + \frac{\tau_{\mathrm{xz}}}{f_{\mathrm{R}}} \leq 1.0 \qquad \frac{\tau_{\mathrm{tor}}}{f_{\mathrm{v,tor}}} + \frac{\tau_{\mathrm{yz}}}{f_{\mathrm{R}}} \leq 1.0 \qquad (11a, 11b)$$

are proposed by Flaig (2015a). The test results indicate a mean value of the torsional strength of about $f_{v,tor}$ = 3.5 MPa and a mean value of the rolling shear strength of about f_R = 1.5 MPa. The corresponding characteristic values are $f_{v,tor,k}$ = 2.75 MPa and $f_{R,k}$ = 1.1 MPa.

3.4 Influence of element lay-up on shear stresses in crossing areas

The parallel to beam axis shear stress τ_{xz} according to Equation (7) and the torsional shear stress τ_{tor} according to Equation (10) are both strongly dependent of the element lay-up in terms of the longitudinal lamination width b and the number m of longitudinal laminations in the beam height direction ($m = h/b$).

According to Flaig (2015a), Equations (7) and (10) give good approximations for the range of lay-ups that are used in practice, also when the ratio $t_{0,k}/n_{CA,k}$ is not constant. Lay-ups with constant value of $t_{0,k}/n_{CA,k}$ for all longitudinal layers are not very common on the market. On the contrary, CLT elements have more often greater longitudinal layer widths in the external layers than in the internal layers. Equations (7) and (10) then underestimate the maximum value of the shear stress parallel to the beam axis and the torsional shear stress.

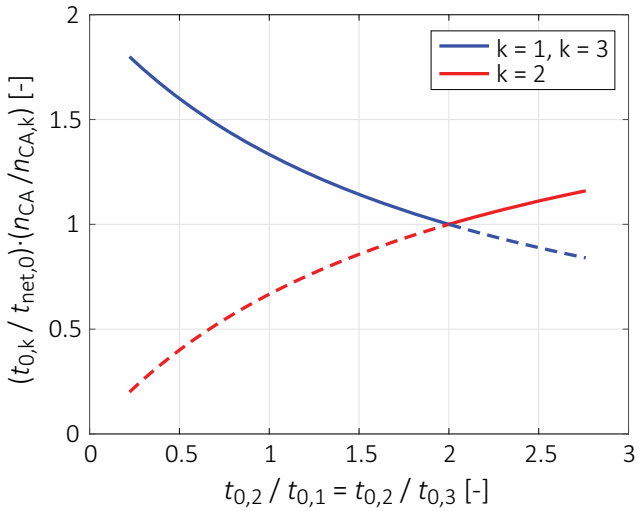

Figure 3.3. Factor for prediction of shear stress vs. relative width of longitudinal layers.

Accounting for varying ratio $t_{0,k}/n_{CA,k}$ between the k layers of longitudinal laminations, the maximum shear stress parallel to the beam axis τ_{xz} and the maximum torsional shear stress τ_{tor} are given by Flaig (2013)

$$\tau_{xz} = \frac{6V}{b^2 n_{CA,k}} \frac{t_{0,k}}{t_{net,0}} \left(\frac{1}{m^2} - \frac{1}{m^3} \right) \tag{12}$$

$$\tau_{tor} = \frac{3V}{b^2 n_{CA,k}} \frac{t_{0,k}}{t_{net,0}} \left(\frac{1}{m} - \frac{1}{m^3} \right) \tag{13}$$

and the difference in predicted stress in the crossing areas belonging to longitudinal lamination k, compared to Equations (7) and (10), may hence be expressed by the factor $(t_{0,k}/t_{net,0})\cdot(n_{CA}/n_{CA,k})$. The relationship between the relative widths of the internal and external layers and the predicted stress for the respective layers is illustrated in Figure 3.3 for a 5-layer CLT element. Assuming a fixed net cross section width $t_{net,0}$, the maximum stress increases by 33 % for the case of equal width of all longitudinal layers and by 60 % for the case of external layers having twice the width of the internal layer, compared to the reference case of $t_{0,2}/t_{0,1} = t_{0,2}/t_{0,3} = 2.0$. Despite this, it is stated in Flaig (2013, 2015a) that for commonly used lay-ups, this influence can be neglected.

4 Test results

The results from the tests, in terms of failure load (maximum load) and maximum values of stress components at the maximum load, are given in Tables 4.1-4.5. The stress values are based on the assumption of equal widths of the longitudinal and transversal laminations according to approximate mean values as $b_0 = b_{90} = b = 150$ mm and of constant ratio $t_{0,k}/n_{CA,k} = t_{net,0}/n_{CA} = 30$ mm for all longitudinal layers. Thus, the influence of the actually varying ratio $t_{0,k}/n_{CA,k}$ has not been taken into account, following the statement of Flaig (Flaig 2013, 2015a) that for commonly used lay-ups this influence is negligible. The stress components corresponding to the dominating mode of failure, based on observations during testing, are indicated by being underlined.

Stress components for test series of beams with a hole (test series A and B) and beams with an end-notch (test series D) are based on models presented by Flaig (2015b). For test series C and E, the respective equation used for calculation of stresses is indicated in the tables by a number in parenthesis. Graphs of applied load *F* vs. beam deflection for the four individual tests of test series A-E are shown in Figure 4.1.

For all tests in series C and E, the load bearing capacity in terms of maximum load is related to bending failure and cracking due to a combination of bending and tension in the longitudinal laminations. Before reaching maximum load, a gradual decrease in stiffness can however be noted from the load vs. deflection graphs for test series E in Figure 4.1. Although the modes of failure are categorized as bending failures, the final failures were for test series E probably preceded by at least partial failure in the crossing areas between longitudinal and transversal laminations before maximum load.

Table 4.1. Failure load (maximum load) and corresponding stress values for test series A.

	F_{max} [kN]	σ_x [MPa]	$\sigma_{x,h}$ [MPa]	$\sigma_{t,0,h}$ [MPa]	$\tau_{xy,gross,h}$ [MPa]	$\tau_{xy,net,90,h}$ [MPa]	$\tau_{xz,h}$ [MPa]	$\tau_{yz,h}$ [MPa]	$\tau_{tor,h}$ [MPa]
A1	277.1	34.6	42.9	18.5	4.33	14.6	0.73	0.62	2.21
A2	295.0	36.9	45.6	19.7	4.61	15.5	0.78	0.66	2.36
A3	293.5	36.7	45.4	19.6	4.59	15.4	0.77	0.65	2.34
A4	304.3	38.0	47.1	20.3	4.76	16.0	0.80	0.68	2.43
Mean	292.5	36.6	45.3	19.5	4.57	15.4	0.77	0.65	2.34

Table 4.2. Failure load (maximum load) and corresponding stress values for test series B.

	F_{max} [kN]	σ_x [MPa]	$\sigma_{x,h}$ [MPa]	$\sigma_{t,0,h}$ [MPa]	$\tau_{xy,gross,h}$ [MPa]	$\tau_{xy,net,90,h}$ [MPa]	$\tau_{xz,h}$ [MPa]	$\tau_{yz,h}$ [MPa]	$\tau_{tor,h}$ [MPa]
B1	523.9	18.2	29.1	20.5	5.46	18.4	0.92	0.68	2.79
B2	475.6	16.5	26.4	18.6	4.95	16.7	0.83	0.62	2.53
B3	491.9	17.1	27.3	19.2	5.12	17.2	0.86	0.64	2.62
B4	502.0	17.4	27.9	19.6	5.23	17.6	0.88	0.65	2.67
Mean	498.3	17.3	27.7	19.5	5.19	17.5	0.87	0.65	2.65

Table 4.3. Failure load (maximum load) and corresponding stress values for test series C.

	F_{max} [kN]	σ_x (1) [MPa]	$\tau_{xy,gross}$ (2) [MPa]	$\tau_{xy,net,0}$ (3) [MPa]	$\tau_{xy,net,90}$ (4) [MPa]	τ_{xz} (7) [MPa]	τ_{yz} (8) [MPa]	τ_{tor} (10) [MPa]
C1	413.2	43.0	3.23	4.30	12.9	0.65	0.37	1.61
C2	363.2	37.8	2.84	3.78	11.3	0.57	0.33	1.42
C3	335.6	35.0	2.62	3.50	10.5	0.52	0.30	1.31
C4	412.9	43.0	3.23	4.30	12.9	0.65	0.37	1.61
Mean	381.2	39.7	2.98	3.97	11.9	0.60	0.35	1.49

Table 4.4. Failure load (maximum load) and corresponding stress values for test seris D.

	F_{max} [kN]	σ_x [MPa]	$\sigma_{x,n}$ [MPa]	$\sigma_{t,0,n}$ [MPa]	$\tau_{xy,gross,n}$ [MPa]	$\tau_{xy,net,90,n}$ [MPa]	$\tau_{yz,n}$ [MPa]	$\tau_{tor,n}$ [MPa]
D1	350.9	29.2	19.5	38.0	5.48	19.6	0.63	2.45
D2	349.3	29.1	19.4	37.8	5.46	19.5	0.63	2.44
D3	361.6	30.1	20.1	39.2	5.65	20.2	0.65	2.53
D4	345.5	28.8	19.2	37.4	5.40	19.3	0.62	2.42
Mean	351.8	29.3	19.5	38.1	5.50	19.7	0.64	2.46

Table 4.5. Failure load (maximum load) and corresponding stress values for test series E.

	F_{max} [kN]	σ_x (1) [MPa]	$\tau_{xy,gross}$ (2) [MPa]	$\tau_{xy,net,0}$ (3) [MPa]	$\tau_{xy,net,90}$ (4) [MPa]	τ_{xz} (7) [MPa]	τ_{yz} (8) [MPa]	τ_{tor} (10) [MPa]
E1	491.3	35.8	3.84	5.12	15.4	0.77	0.44	1.92
E2	519.5	37.9	4.06	5.41	16.2	0.81	0.47	2.03
E3	513.0	37.4	4.01	5.34	16.0	0.80	0.46	2.00
E4	476.3	34.7	3.72	4.96	14.9	0.74	0.43	1.86
Mean	500.0	36.5	3.91	5.21	15.6	0.78	0.45	1.95

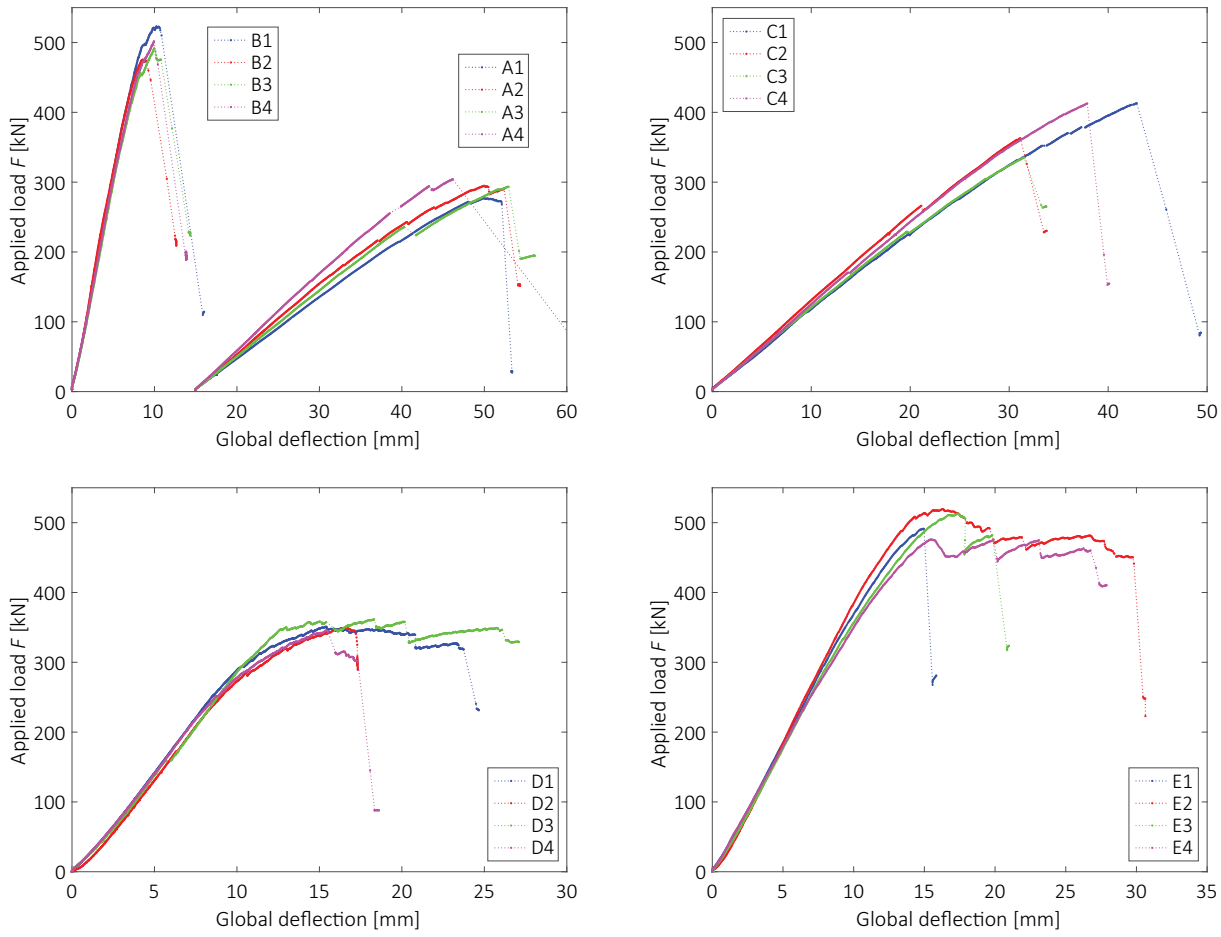

Figure 4.1. Applied load F vs. global beam deflection for test series A, B, C, D and E.

5 FE-analysis

3D FE-analyses were carried out in order to investigate the influence of the relative width of the longitudinal layers $t_{0,k}$ on the shear stresses in the crossing areas as discussed in Section 3.4. Also the distribution of $M_{tor,i,k}$ with respect to the beam height direction was investigated, this being relevant in relation to Equations (10) and (13).

The FE-analyses were performed using Abaqus 2017. The laminations were modelled as linear elastic and orthotropic with stiffness parameters according to Table 5.1. The rectilinear material directions are denoted by *L* in the lamination length direction, *T* in the width direction and *R* in the thickness direction. Adjacent laminations within the same layer were modelled with a 0.1 mm gap. The flatwise bonding between the laminations was modelled using a combination of hard contact in compression and elastic response in tension perpendicular to the crossing areas and in the two shear directions. The linear elastic traction-separation model used a single stiffness value for all three directions, $K_{nn} = K_{tt} = K_{ss} = 1000$ N/mm^3, for tension and the two shear directions, respectively. The contact stiffness parameters were chosen based on comparison of calculated global beam stiffness according to the FE-model and the experimentally found beam stiffness (values in the range of 10-1000 N/mm^3 were tested, showing negligible influence on the force distribution and minor influence on global stiffness).

A gross beam geometry and loading situation according to test series C, see Figure 2.1, was used considering symmetry in two directions. 8-node linear brick elements (C3D8 in Abaqus) was used and the FE-meshes consisted of cubically, or close to cubically, shaped elements having a side length of about 10 mm. Longitudinal and transversal laminations widths were assigned as $b_0 = b_{90} = 150$ mm and the applied load corresponds to $V = 0.5F = 100$ kN. Three beam lay-ups were considered, according to:

- Lay-up 30-20-60-20-30 ($t_{net,0} = \Sigma t_{0,k} = 120$ mm, $t_{0,2}/t_{0,1} = t_{0,2}/t_{0,3} = 2.0$)
- Lay-up 40-20-40-20-40 ($t_{net,0} = \Sigma t_{0,k} = 120$ mm, $t_{0,2}/t_{0,1} = t_{0,2}/t_{0,3} = 1.0$)
- Lay-up 48-20-24-20-48 ($t_{net,0} = \Sigma t_{0,k} = 120$ mm, $t_{0,2}/t_{0,1} = t_{0,2}/t_{0,3} = 0.5$)

Internal forces and moments found from the FE-analyses and according to the analytical model presented by Flaig and Blass are presented in Tables 5.2-5.4, considering forces and moments as illustrated in Figure 5.1. The forces from the FE-analyses are determined by integration of stresses in the longitudinal laminations and in the crossing areas, respectively. The forces from the analytical model are determined based on the actual ratio $t_{0,k}/n_{CA,k}$. The influence of element size was tested for one beam lay-up, showing negligible influence on force distributions even with element size of 5 mm.

Table 5.1 Lamination stiffness parameters used for FE-analyses.

E_L	E_T	E_R	G_{LT}	G_{LR}	G_{TR}	ν_{LT}	ν_{LR}	ν_{TR}
[MPa]	[MPa]	[MPa]	[MPa]	[MPa]	[MPa]	[-]	[-]	[-]
12000	400	600	750	600	75	0.50	0.50	0.33

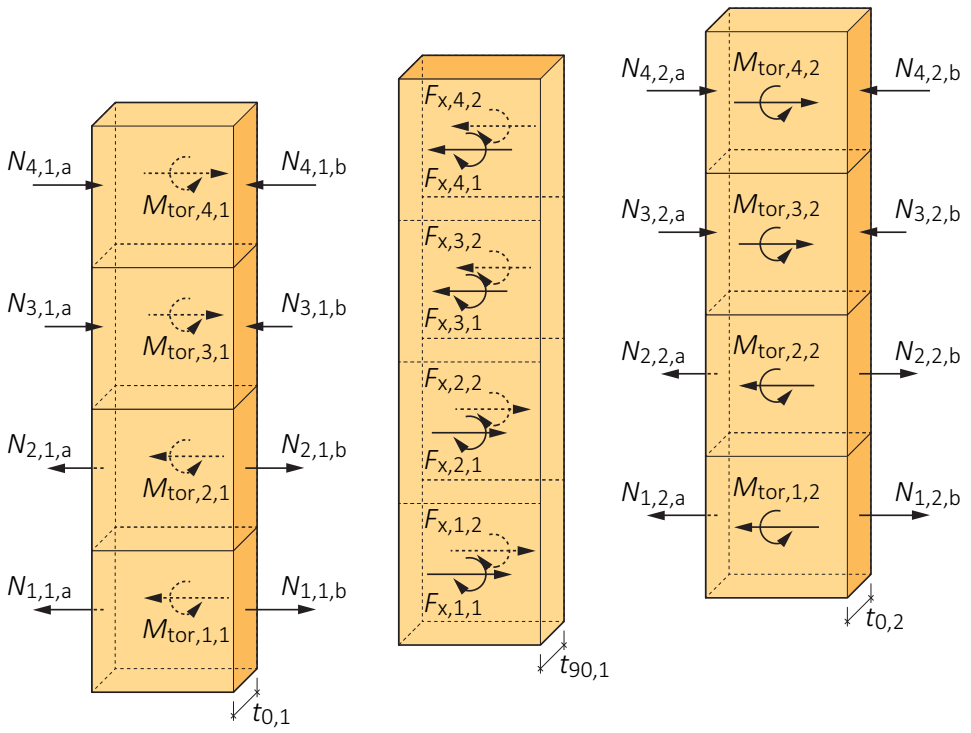

Figure 5.1. Internal forces/moments $N_{i,k}$, $F_{x,i,k}$ and $M_{tor,i,k}$ in longitudinal/transversal laminations.

The internal forces $N_{i,k}$ and $F_{x,i,k}$ as calculated by the analytical model and by FE-analyses agree well in general, however showing slightly larger discrepancies for $F_{x,i,k}$ compared to $N_{i,k}$. Regarding the torsional moments $M_{tor,i,k}$, the agreement between the analytical model and the FE-results is less good with differences being in the range of ± 50 % and even more. The absolute values of $F_{x,i,k}$ and $M_{tor,i,k}$ from the FE-analyses were found to be sensitive to the method of evaluation, i.e. the post-processing approach used for integration of stresses. The relative magnitude between the layers (i.e. the relative load sharing between layers) was however not much affected.

Table 5.2. Internal forces, in N, and torsional moments, in Nmm, for lay-up 30-20-60-20-30.

	$N_{i,1,a}$		$N_{i,1,b}$		$F_{x,i,1}$		$M_{tor,i,1}$	
i	FE	Analytical	FE	Analytical	FE	Analytical	FE	Analytical
4	28200	28100	34800	35100	7140	7030	607000	879000
3	9490	9360	11300	11700	1920	2340	1220000	879000
2	9580	9360	11500	11700	2060	2340	1180000	879000
1	28100	28100	34500	35100	7000	7030	489000	879000
	0.5 $N_{i,2,a}$		0.5 $N_{i,2,b}$		$F_{x,i,2}$		$M_{tor,i,2}$	
i	FE	Analytical	FE	Analytical	FE	Analytical	FE	Analytical
4	28200	28100	34800	35100	7150	7030	604000	879000
3	9480	9360	11200	11700	1930	2340	1220000	879000
2	9590	9360	11500	11700	2060	2340	1180000	879000
1	28100	28100	34500	35100	7010	7030	487000	879000

Table 5.3. Internal forces, in N, and torsional moments, in Nmm, for lay-up 40-20-40-20-40.

	$N_{i,1,a}$		$N_{i,1,b}$		$F_{x,i,1}$		$M_{tor,i,1}$	
i	FE	Analytical	FE	Analytical	FE	Analytical	FE	Analytical
4	37600	37400	46300	46800	9370	9380	693000	1170000
3	12600	12500	14900	15600	2510	3130	1380000	1170000
2	12800	12500	15300	15600	2690	3130	1330000	1170000
1	37500	37400	46000	46800	9200	9380	540000	1170000
	0.5 $N_{i,2,a}$		0.5 $N_{i,2,b}$		$F_{x,i,2}$		$M_{tor,i,2}$	
i	FE	Analytical	FE	Analytical	FE	Analytical	FE	Analytical
4	18800	18700	23300	23400	4880	4690	517000	586000
3	6350	6240	7560	7800	1330	1560	1050000	586000
2	6370	6240	7670	7800	1420	1560	1020000	586000
1	18700	18700	23100	23400	4790	4690	435000	586000

Table 5.4. Internal forces, in N, and torsional moments, in Nmm, for lay-up 48-20-24-20-48.

	$N_{i,1,a}$		$N_{i,1,b}$		$F_{x,i,1}$		$M_{tor,i,1}$	
i	FE	Analytical	FE	Analytical	FE	Analytical	FE	Analytical
4	45200	44900	55500	56200	11200	11300	782000	1410000
3	15100	15000	17800	18700	2980	3750	1540000	1410000
2	15400	15000	18300	18700	3190	3750	1480000	1410000
1	45000	44900	55100	56200	11000	11300	599000	1410000
	0.5 $N_{i,2,a}$		0.5 $N_{i,2,b}$		$F_{x,i,2}$		$M_{tor,i,2}$	
i	FE	Analytical	FE	Analytical	FE	Analytical	FE	Analytical
4	11300	11200	14000	14000	3000	2810	427000	352000
3	3830	3740	4570	4680	825	938	870000	352000
2	3810	3740	4610	4680	885	938	849000	352000
1	11300	11200	13900	14000	2950	2810	373000	352000

6 Discussion and conclusions

Based on the present tests of prismatic beams and beams with a hole or an end-notch, considering the results in terms of stress components as presented in Tables 4.1-4-5, and strength values according to Section 3.3, the model suggested by Flaig (2015a, 2015b) seems to yield reasonable or conservative predictions for the beam strength.

As regards shear failure in the crossing areas (shear mode III) and Equations (5)-(10), the considered model is derived based on assumptions of constant ratio $t_{0,k}/n_{CA,k}$ for all longitudinal layers and is hence for 5- and 7-layer CLT elements (strictly) valid only when having internal longitudinal layer/layers of twice the width as the external longitudinal layers. Furthermore, equal width of the longitudinal and transversal laminations according to $b_0 = b_{90} = b$ is assumed. The present specimens were composed of

elements with varying ratio $t_{0,k}/n_{CA,k}$ and different laminations widths for the longitudinal and transversal layers. Also the width of the individual longitudinal laminations differed within the specimens, with the widths of the upper- and lower-most longitudinal laminations being in the range 5 mm < b_0 < 172 mm. Despite the discrepancies between model assumptions and present specimen geometries, reasonable or conservative predictions for the beam strength were found.

The comparison of results according to the FE-analyses and the analytical expressions, in terms of the lamination forces $F_{x,i,k}$ and $N_{i,k}$ according to Tables 5.2-5.4, show overall a reasonable agreement. Comparing lay-ups 40-20-40-20-40 and 48-20-24-20-48 to the lay-up 30-20-60-20-30, the results of the FE-analyses for $F_{x,i,k}$ agree well with the influence of the ratio $t_{0,k}/n_{CA,k}$ as predicted by Equation (12) and shown in Figure 3.3. Thus, it seems that, at least for the cases investigated here, the approach used by Flaig to determine these lamination *forces* is adequate, *taking into account the influence of the lamination width ratio* $t_{0,k}/n_{CA,k}$, which cannot be neglected.

The FE-analyses also showed that the torsional moments $M_{tor,i,k}$ are influenced by the ratio $t_{0,k}/n_{CA,k}$, although not to the full extent as predicted by Equation (13) and shown in Figure 3.3. Comparing lay-ups 40-20-40-20-40 and 48-20-24-20-48 to the lay-up 30-20-60-20-30, the FE-analyses give about 13 % and 26 % increase in torsional moments. The assumption that the torsional moments are equal for all crossing areas in the beam height direction is clearly not supported by the FE-analyses, see Tables 5.2-5.4, which show significantly higher torsional moments close to the beam central axis.

Table 6.1 shows the mean values of estimated shear stresses from test series C and E assuming either a constant, or the actual, ratio $t_{0,k}/n_{CA,k}$ and evaluation of Equation (11a) based on proposed mean values of $f_{v,tor}$ = 3.5 MPa and f_R = 1.5 MPa. The final failure for all tests of both test series C and E was categorized as bending failure. From this comparison, it appears as is if the mean shear strengths $f_{v,tor}$ and f_R of the beams tested are greater than the assumed mean values. For test series E, the gradual decrease in stiffness prior to reaching maximum load may however be due to partial failure/damage in the crossing areas. Another possible reason for the comparatively high stress interaction ratios, without obvious shear mode III failure, may be that the assumption of equal torsional moments for all crossing areas in the beam height direction is inaccurate, as suggested by the FE-analyses.

Table 6.1. Estimated mean shear stress at failure (shear mode III) and evaluation of Equation (11a).

	$t_{0,k}/n_{CA,k} = t_{net,0}/n_{CA}$ = 30 mm			$t_{0,k}/n_{CA,k}$ = 40 mm		
	τ_{xz} (7) [MPa]	τ_{tor} (10) [MPa]	Interaction (11a) [-]	τ_{xz} (12) [MPa]	τ_{tor} (13) [MPa]	Interaction (11a) [-]
Test series C	0.60	1.49	0.83	0.79	1.99	1.10
Test series E	0.78	1.95	1.08	1.04	2.60	1.44

It should be noted that, from a theoretical point of view, the origin of the in-plane shear stress components acting in the crossing areas is irrelevant. The "torsional shear strength", $f_{v,tor}$, can thus only be understood as a fictitious strength parameter strongly related to the structural properties of the test conditions used to determine it.

7 Acknowledgments

The financial support from the Swedish Research Council Formas through grant 2016-01090 and from COST Action FP1402 (for the Short Term Scientific Mission (STSM) of Mario Jeleč to Lund University during the fall of 2016) is gratefully acknowledged.

8 References

Abaqus 2017 (2016), Dassault Systèmes.

Andreolli M, Tomasi R, Polastri A (2012): Experimental investigation on in-plane behaviour of cross-laminated timber elements. In: Proc. CIB-W18, CIB-W18/45-12-4, Växjö, Sweden.

Bejtka I (2011): Cross (CLT) and diagonal (DLT) laminated timber as innovative material for beam elements. KIT, Karlsruhe, Germany.

Danielsson H, Jeleč M, Serrano E (2017): Strength and stiffness of cross laminated timber at in-plane beam loading. Report TVSM-7164, Division of Structural Mechanics, Lund University, Sweden.

European Technical Assessment ETA-15/0906 from 24.02.2016. Cross Timber Systems – CLT, Solid wood slab elements to be used as structural elements in buildings. Austrian Institute for Construction Engineering, Vienna, Austria.

Flaig M (2013): Biegeträger aus Brettsperrholz bei Beanspruch in Plattebene. PhD thesis, KIT, Karlsruhe, Germany.

Flaig M, Blass HJ (2013): Shear strength and shear stiffness of CLT-beams loaded in plane. In: Proc. CIB-W18, CIB-W18/46-12-3, Vancouver, Canada.

Flaig M (2014): Design of CLT beams with rectangular holes or notches. In: Proc. INTER, INTER/47-12-4, Bath, United Kingdom.

Flaig M (2015a): In Plattenebene beanspruchte Biegeträger aus Brettsperrholz – Teil 1: Effektive Festigkeits- und Steifigkeitskennwerte für die Schubbemessung. Bautechnik 92:741-749.

Flaig M (2015b): In Plattenebene beanspruchte Biegeträger aus Brettsperrholz – Teil 2: Brettsperrholzträger mit angeschnittenen Rändern, Durchbrüchen oder Ausklinkungen. Bautechnik 92:750-758.

Jeleč M, Rajčić V, Danielsson H, Serrano E (2016): Structural analysis of in-plane loaded CLT beam with holes: FE-analysis and parameter studies. In: Proc. INTER, INTER/49-12-2, Graz, Austria.